Ionics (2021) 27:97–105
https://doi.org/10.1007/s11581-020-03785-1

ORIGINAL PAPER

Nitrogen–phosphorus co-doped porous carbon using ionic liquids as a dual functional agent for high-performance long-life lithium ion batteries

Ying-xue Guo[1] · Yan-shuang Meng[1,2] · Yue-yong Du[1] · Ming-tao Duan[1] · Yu-zhu Li[1] · Fu-liang Zhu[1,2]

Received: 24 April 2020 / Revised: 20 August 2020 / Accepted: 12 September 2020 / Published online: 25 September 2020

Abstract

A new kind of nitrogen–phosphorus co-doped porous carbon (NPPC) material was prepared by using ionic liquids as a dual functional agent and KCl and $ZnCl_2$ as a salt template. Scanning electron microscopy and transmission electron microscopy images demonstrated that the NPPC material has a uniform porous structure with a high specific surface area of 589.97 $m^2\ g^{-1}$. When the NPPC material used as anode materials for lithium-ion batteries, thanks to its good pore structure (contain rich mesoporous and macroporous) and successful doping of nitrogen and phosphorus (9.12 and 0.28 at.%, respectively), its initial discharge capacity is up to 685 mAh g^{-1} at a current density of 0.1 A g^{-1}. After 50 cycles, reversible capacity of NPPC stays around 715 mAh g^{-1} and the coulomb efficiency remained above 97%. After 400 cycles at the current density of 2 A g^{-1}, the capacity can still maintain at 394.1 mAh g^{-1}. All results show that the NPPC material has excellent electrochemical properties that can be viewed as a promising candidate for anode materials in lithium-ion batteries.

Keywords Nitrogen-phosphorous co-doping porous carbon · Salt template · Ionic liquids · Lithium-ion batteries

Introduction

As an energy storage system, rechargeable lithium ion batteries (LIBs) have been widely used in portable electronic devices due to their high energy density, long cycle life, and high safety performance compared with other batteries, for instance, nickel–cadmium batteries and nickel–metal hydride batteries. In recent years, the application of LIBs has been extended to large electronic vehicles, whereas the common anode materials cannot meet the needs of LIBs [1–4]. Graphite is the most commonly used industrial anode material; however, its theoretical capacity is only 372 mAh g^{-1}, limiting its cycling properties and rate performance [5, 6]. Therefore, efforts have been made to find new carbon-based anode materials to improve the storage capacity of lithium ions.

The structure of materials has become a chief research object. After studying the carbon anode materials with different microstructures, such as carbon nanotubes [7], nanofibers [8], nanorods [9], hollow nanospheres [10], graphene [11], and porous carbon [12], porous carbon is considered to be the most promising anode material for LIBs. This can be attributed to the fact that porous carbon materials have micropores and mesoporous pores, which can shorten the transport distance of lithium ions and provide the interface of electrode electrolyte to promote the charge reaction, so as to make them have high lithium capacity and good cycling stability [13–15]. Because of the recognition of porous carbon materials, a variety of methods for preparing them have emerged.

Among those methods, the most widely used are soft template method, hard template method, and chemical physical activation method [16, 17]. The soft template method has high controllability in pore structure and pore size distribution, and the synthesized porous carbon electrode can show good electrochemical performance. For example, Wang et al. prepared nitrogen-doped porous carbon microtubes by soft template method, which showed high reversible capacity (877.3 mAh g^{-1} at 0.05 A g^{-1}) and good rate performance (251.1 mAh g^{-1}

✉ Fu-liang Zhu
chzfl@126.com

[1] School of Materials Science and Engineering, Lanzhou University of Technology, Lanzhou 730050, China

[2] State Key Laboratory of Advanced Processing and Recycling of Non-ferrous Metals, Lanzhou University of Technology, Lanzhou 730050, China

at 5 A g^{-1}) [6]. However, only a few carbon precursors were suitable for this standard, such as phloroglucinol, resorcinol, and formaldehyde. Chemical activation and hard formwork methods can avoid shortages of raw materials. Jia et al. prepared graded porous carbon with continuous nonwoven glass fiber as template, glucose as precursor, and KOH as activator, which has high specific capacitance and good cyclic stability [18]. However, many researchers use activators and corrosion solutions such as sodium hydroxide, potassium hydroxide, or hydrofluoric acid in the preparation of final products. These are usually toxic and polluting chemicals, which are major drawbacks that have seriously hindered the commercialization of chemical activation methods. In recent years, the nanocasting method with silica as the skeleton has been widely used in the preparation of porous carbon materials. But this method is very complicated and the carbonization conditions are harsh, which is difficult to adapt to the preparation of large-scale ordered nano-porous carbon films or monolithic stones [19, 20]. Therefore, it is worthwhile to study how to synthesize porous carbon easily, cheaply, and environmentally. Potassium chloride (KCl) and zinc chloride ($ZnCl_2$) are environmentally friendly and low-cost compounds that can be used as hard templates. After carbonization, they are easy to be erased by water and the residue is kept at a low level. Most notably, both compounds are freely soluble in water, which means they can be uniformly dispersed in carbon precursor solutions [21].

Apart from the structure, a number of studies were demonstrated that the electrochemical properties of the carbon-based anode could be further improved by doping with heteroatoms [22–24]. When it comes to single atom doping, nitrogen as a "neighbor" of carbon is the most abundantly investigated heteroatom up to now. The incorporation of nitrogen atoms leads to more defects in the external structure as the available active site, enhancing the electrochemical reactivity and conductivity, thus making a significant contribution to the superior reversible capacity, rate performance, and cycling stability performance of the LIBs [25–27]. Nevertheless, in recent years, researchers pay an increasing number of attentions to the study of binary doping and ternary doping. Cai and his team proposed a method for synthesizing nitrogen (N) and sulfur (S) co-doped graphene sheets, which had a reversible capacity of 250 mAh g^{-1} when the current density was 20 A g^{-1} [28]. Choi and his co-worker reported that the ternary doping of B and P with N into the carbon structure, the results showed that the co-doping of N, B, and P produced a structure with more edge sites so that its catalyst activity was 2.3 times higher than the material doped only with nitrogen [29]. Many researchers have found that carbon materials with nitrogen and phosphorus co-doping have great potential. The nitrogen–phosphorus co-doped porous carbon material prepared by Wang et al. has an adjustable surface base with uniform pores, so it has good electrochemical performance in supercapacitors [30]. Jiang et al. developed a nitrogen–phosphorus co-doped fractionated porous carbon foam material as an efficient metal-free catalyst for ORR. The sample obtained has excellent catalytic activity in alkaline, neutral, and acidic media. In addition, compared with the most advanced Pt/C catalyst in the commercial market, it has better methanol oxidation resistance and higher stability [31]. It has been proved that the good properties of nitrogen and phosphorus co-doped materials can be attributed to the following two points. On the one hand, the effect of phosphorus can promote charge separation and enhance conductivity [32]. On the other hand, the synergistic effect of N and P atoms can help to improve the capacitance of material. The reason is that the electronegativity of C, N, and P element are about 2.55, 3.04, and 2.19, respectively, so the charge in the carbon skeleton is redistributed, and more charge is transferred from the carbon atoms to the nearby nitrogen and phosphorus atoms [29, 33]. At present, there are a few researches on the application of nitrogen and phosphorus co-doping in lithium ion batteries.

In this work, we demonstrate a simple and effective method for the preparation of nitrogen-phosphorus co-doped porous carbon materials using KCl and $ZnCl_2$ as salt template for lithium ion batteries. NPPC is prepared by salt template method using ionic liquid 1-ethyl-3-methylimidazolium dicyanamide and 1-butyl-3-methylimidazolium hexafluorophosphate as the carbon source and doping agent. It is worth noting that the unique solvation environment offered by ionic liquids can make heteroatoms evenly doped in the sample. The electrochemical properties of NPPC show that this material is not only beneficial to the rapid transport of ions and electrons but also improves the capacitive contribution. So that it has fantastic reversibility, rate performance, and cyclic stability.

Experimental section

Materials

Potassium chloride (99 wt%) and zinc chloride (99 wt%) were purchased from Aladdin Reagent Co. Ltd. (Shanghai, China). 1-Ethyl-3-methylimidazolium dicyanamide and 1-butyl-3-methylimidazolium hexafluorophosphate were obtained from Lanzhou Institute of Chemical Physics. All the other chemicals and reagents were analytical grade and used without further refinement.

Synthesis of nitrogen and phosphorus co-doped porous carbon

The sample is directly carbonized by a mixture of ionic liquid and salt template. The mass ratio of 1-Ethyl-3-methylimidazolium dicyanamide to 1-butyl-3-

methylimidazolium hexafluorophosphate is 1:4.5, and the mass ratio of KCl and $ZnCl_2$ is 1:1. The mixture is well mixed by full grinding; then, the mixture was put into a tube furnace filling with argon gas and carbonized at 800 °C for 1 h with a heating rate of 5 °C min^{-1}. Finally, the sample was washed in deionized water and hydrochloric acid and dried in a vacuum. Finally, nitrogen–phosphorus co-doped porous carbon was obtained.

Materials characterization

X-ray diffraction (XRD) patterns were recorded on a Bruker D8 Advance diffractometer using Cu Ka radiation. X-ray photoelectron spectroscopy (XPS) studies were carried out on an Escalab 250Xi. The surface morphology and microstructure of the sample were observed from scanning electron microscopy (SEM, JSM-6701F) and transmission electron microscopy (TEM, JEM-2010F, JEOL, Japan). Raman spectra of the composite were collected on a Lab RAM HR UV/vis/NIR (Honba Jobin Yvon, France). The nitrogen adsorption–desorption curves were registered on an ASAP-2020 (Micromeritics Instrument Crop, America) analyzer isothermally at 77 K. The specific surface area of NPPC was calculated by applying Brumaire-Emmett-Teller (BET) method, and the pore size distributions were determined by the adsorption branch using Barrett–Joyner–Halenda (BJH) method.

Electrochemical measurements

CR2032 coin-type cell with a charge–discharge system was used to test the electrochemical performance. The anode electrodes were prepared by mixing the active material, acetylene black, and polyvinylidene fluoride (PVDF) in a weight ratio of 8:1:1 in N-methyl pyrrolidinone (NMP) until homogeneous slurry was obtained in mortar. After that coating the synthetic slurry on the copper foil uniformly and dried in a vacuum drying oven for 12 h at 80 °C subsequently. Lithium foil and a polypropylene micro-porous film were used as the opposite electrode and the separator respectively. The electrolyte used 1M $LiPF_6$ in a mixture of ethylene carbonate (EC) and 1,2-dimethoxyethane (DEC) with a volume ratio of 1:1. The coin-type test cells were assembled in an argon-filled glove box and then stood for 24 h. Within the potential confines of 0.01 to 3.0 V, the coin-type test cells were galvanostatically charged and discharged at 0.1 A g^{-1}. The rate performance test was tested at different current densities of 0.1 A g^{-1}, 0.2 A g^{-1}, 0.5 A g^{-1}, 1 A g^{-1}, and 5 A g^{-1}, respectively, and decreased to 0.1 A g^{-1} once again. The cyclic voltammetry (CV) and the electrochemical impedance spectroscopy (EIS) were carried out using a CHI 660E electrochemical workstation.

Result and discussion

The morphology of the prepared materials was observed by SEM and TEM; as shown in Fig. 1a, the SEM images clearly show the resulting nitrogen–phosphorus co-doped carbon material is composed of spherical nanoparticles, leading to generate a rough and irregular surface. After zooming in on Fig. 1a, we can precisely observe from Fig. 1b that these particles are about 20–50 nm in diameter. The spherical nanoparticles are conductive to enhance the rate performance. As can be seen from Fig. 1c, the carbon distribution of the prepared

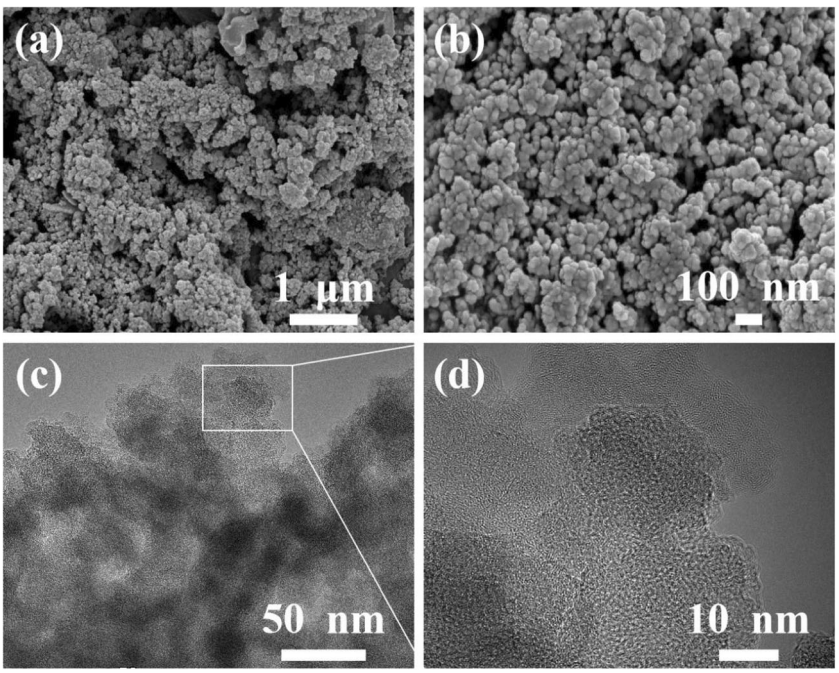

Fig. 1 The SEM (**a**,**b**) and TEM (**c**,**d**) images of NPPC

samples is uniform, which also indicates that the water solubility of KCl and $ZnCl_2$ has a great contribution. Local magnification of Fig. 1c is showed by Fig. 1d; we can clearly see that the pores in the material are evenly distributed with a large number, which proves that the material we prepared is indeed a porous carbon structure. The porous structures can lessen the transport distance of lithium ions to facilitate the rapid diffusion of lithium ions and provide a great electrode/electrolyte interface for charge transfer reactions [34–36].

Raman spectroscopy measurements, which presented in Fig. 2a, were conducted to further study the structure of the carbon samples. The results exhibit two well-defined peaks centered at about 1348 cm^{-1} and 1595 cm^{-1}, which correspond to the D (defect) band that in connection with the disordered arrangement of carbon materials and the G (graphite) band that is relevant to the well-organized graphitic structure of carbon, respectively [37, 38]. The intensity ratio of D band to G band (I_D/I_G) can generally be of help to evaluate the disordered degree of carbon [39]. The I_D/I_G value of NPPC material is 0.845, suggesting that the composite samples have many defects and vacancies, which is thanks to the doped nitrogen and phosphorus [40, 41]. A mass of defects or disorders introduced in NPPC is in favor of the storage and diffusion of lithium. Therefore, the electrochemical properties can also be improved [42].

The XRD patterns of NPPC are shown in Fig. 2b. The typical diffraction humps at 25°, corresponding to the (002) plane of graphitic carbon [43]. The diffraction peak of the salt template cannot be observed from XRD, indicating that there is no residuary salt template in NPPC [34].

To further determine the pore structure and porosity of NPPC materials, the N_2 adsorption–desorption experiment was performed and the curves are exhibited in Fig. 2c. According to IUPAC classification [44], it can be seen that the NPPC accordance with a typical type II curve, implying the existence of some mesopores and macropores in carbon material. This consequence is coincided with the observation from SEM. Figure 2 d is corresponding pore size distribution. As the figure shown, the pore sizes are centered at 2 and 150 nm, including micropores, mesopores, and macropores. To a certain extent, the increase of the fast transport channels of electron and ion and rapid diffusion of electrolyte are attributed to the abundance of mesoporous [45].

In order to investigate the doping state of nitrogen and phosphorus, the existential form of elements, and functional groups on the surface of the carbon sample, XPS analysis was carried out in detail. Figure 3 a shows there are C, N, O, and P elements existed in NPPC. Simultaneously, it demonstrates the prominent peak of C 1s, O 1s, and N 1s and the relatively weak peak of P 2p at 284.43 eV, 531.39 eV, 399.05 eV, and 139.47 eV, respectively. In the high-resolution XPS spectra of C 1s (Fig. 3b), the peaks at 284.82, 285.7, 287.08, and 290.37 eV severally belong to C–O, C–N/C–O–P, C–O, and C=O bond [46, 47]; testifying N and P heteroatoms were successfully incorporated into the sample. For the N 1s region, the spectra can be separated out three peaks (Fig. 3c), the peak at 398.47 eV represents pyridinic N, the peak at 399.1 eV corresponds to pyrrolic N, and the peak at 400.82 eV is assigned to graphitic N [33, 48]. As a rule, pyrrolic N and pyridinic N are taken shape at the edges or defects of carbon materials, which introduces more synthetic defects to carbon materials as the active sites of electrochemistry; there is no denying that they play an essential role in enhancing the performance of capacity [49]. In addition, the graphite nitrogen can reduce the electronic transport resistance to improve the conductivity; hence, the battery dynamics could be

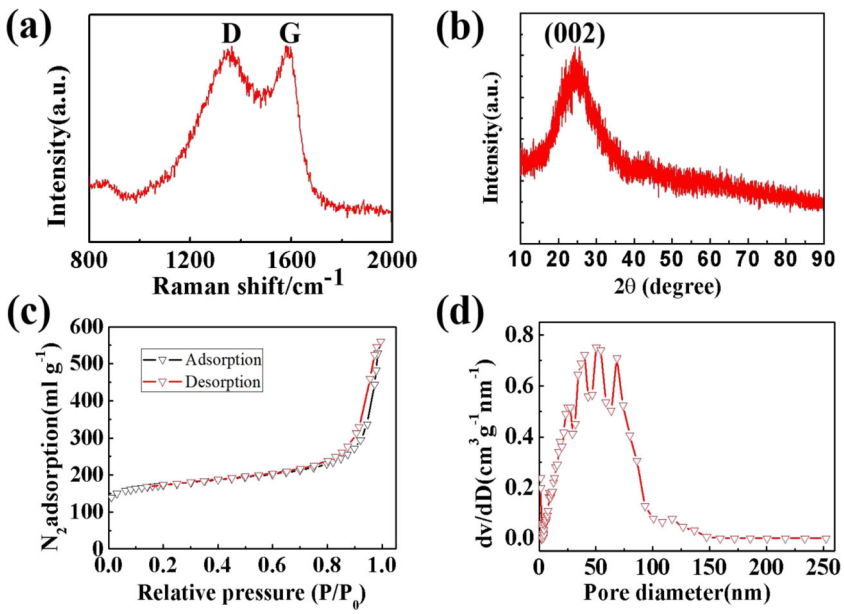

Fig. 2 **a** Raman spectrum, **b** XRD pattern, **c** N_2 adsorption-desorption isotherm curves, and **d** the corresponding pore size distributions plots of NPPC

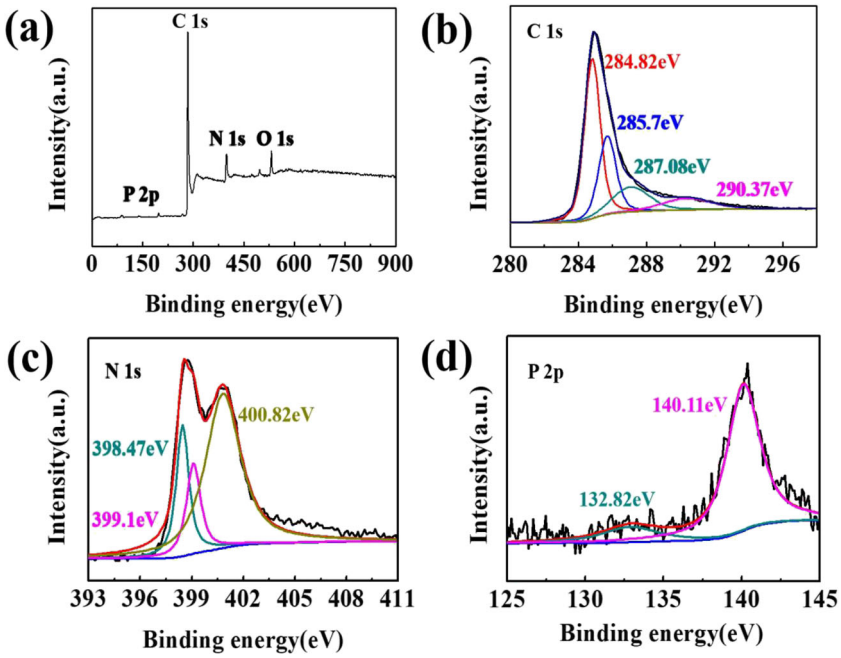

Fig. 3 **a** XPS survey spectrum of NPPC. High-resolution XPS spectra of C 1s (**b**), N 1s (**c**), and P 2p (**d**)

strengthened [50, 51]. Concerning to P 2p, the spectrum contains two fitted peaks at 130.82 eV and 140.11 eV (Fig. 3d), the low binding energy peak corresponds to P–C bond that verifying Phosphorus atoms are present in the carbon lattice [52], and the high binding energy peak corresponds to bond. The successful P doping is deemed to the benefit of improving capacitance, which can be attributed to phosphorus atoms have lower electronegativity and larger radii than carbon to in favor of generating more structural defects; therefore, more active sites are provided [24, 53].

In order to further get a clear understanding of the potential application value of the prepared materials in lithium batteries, electrochemical performance testing was carried out as shown in Fig. 4. Figure 4 a exhibits the rate capabilities of the prepared sample, which is evaluated at current densities in the range from 0.1 to 5 A g^{-1}. Reversible capacities of 685 mAh g^{-1}, 610 mAh g^{-1}, 518 mAh g^{-1}, 372 mAh g^{-1}, and 155 mAh g^{-1} are obtained at 0.1A g^{-1}, 0.2 A g^{-1}, 0.5 A g^{-1}, 1 A g^{-1}, and 5 A g^{-1}, respectively. When the current density restores to 0.1 A g^{-1}, the reversible capacity of NPPC maintains at 695 mAh g^{-1}; this relatively high data attests NPPC has benign rate and reversibility properties. Figure 4 b shows the cycling performance of NPPC electrode tested under a long-term cycling up to 50 cycles at 0.1 A g^{-1}. After 50 cycles, the reversible capacity of NPPC stays around 715 mAh g^{-1} and the coulomb efficiency remained above 97%. The reason for this satisfactory outcome is that the porous carbon structure is conductive to shorten the transport distance of lithium ions [39]. Figure 4 c is the charge and discharge curves of NPPC at the initial three times, which is used to evaluate the electrochemical lithium storage performance of the electrode. During the first cycle, it is observed that NPPC delivers a high initial discharge specific capacity of 1189.2 mAh g^{-1} and a high reversible capacity of 720.4 mAh g^{-1} is achieved, which is about twice times as much as commercial graphite [54]. In the second cycle, the discharge specific capacity and reversible capacity decreased to 750.5 mAh g^{-1} and 693.3 mAh g^{-1}, respectively. The large capacity loss is mainly due to the formation of solid electrolyte interface (SEI) and secondary reactions [55]. In the subsequent cycles, both discharge-specific capacities and reversible capacities of NPPC tend to stable, certifying a superior Li^+ storage performance. In order to study the electrochemical process and understand the possible way of charge storage to account for the high rate property of NPPC, we used cyclic voltammetry to test the sample in the potential range from 0.05 to 3 V at the scanning rate of 0.1 mV s^{-1}. The first three CV curves obtained are shown in the Fig. 4d. It can be seen that the CV curve is not rectangular at high potential, indicating that there is no storage behavior of capacitive lithium, which means it is more suitable for practical application [6]. In the first scan, the obvious reduction peaks are monitored between 0.55 and 0.85 V, which on account of the decomposition of the electrolyte and the formation of SEI films [7]. The reason why there is a peak close to 0 V in the CV curves is that the insertion of lithium ions into the carbon layer. In the anode scan, there is a broad oxidation peak at 0.2 V, which is ascribed to the extraction of lithium from the carbon layer. The result is in accord with previous observations about lithium storage in nitrogen-doped porous carbon materials [56]. Meanwhile, the peak at 1.1 V is also regarded as an oxidation peak, which results from the lithium extraction from defects, for instance, pores, edges, and corners of the carbon layers [6]. From the second cycle, it is not hard to see that the CV curves nearly overlap, which on the one hand

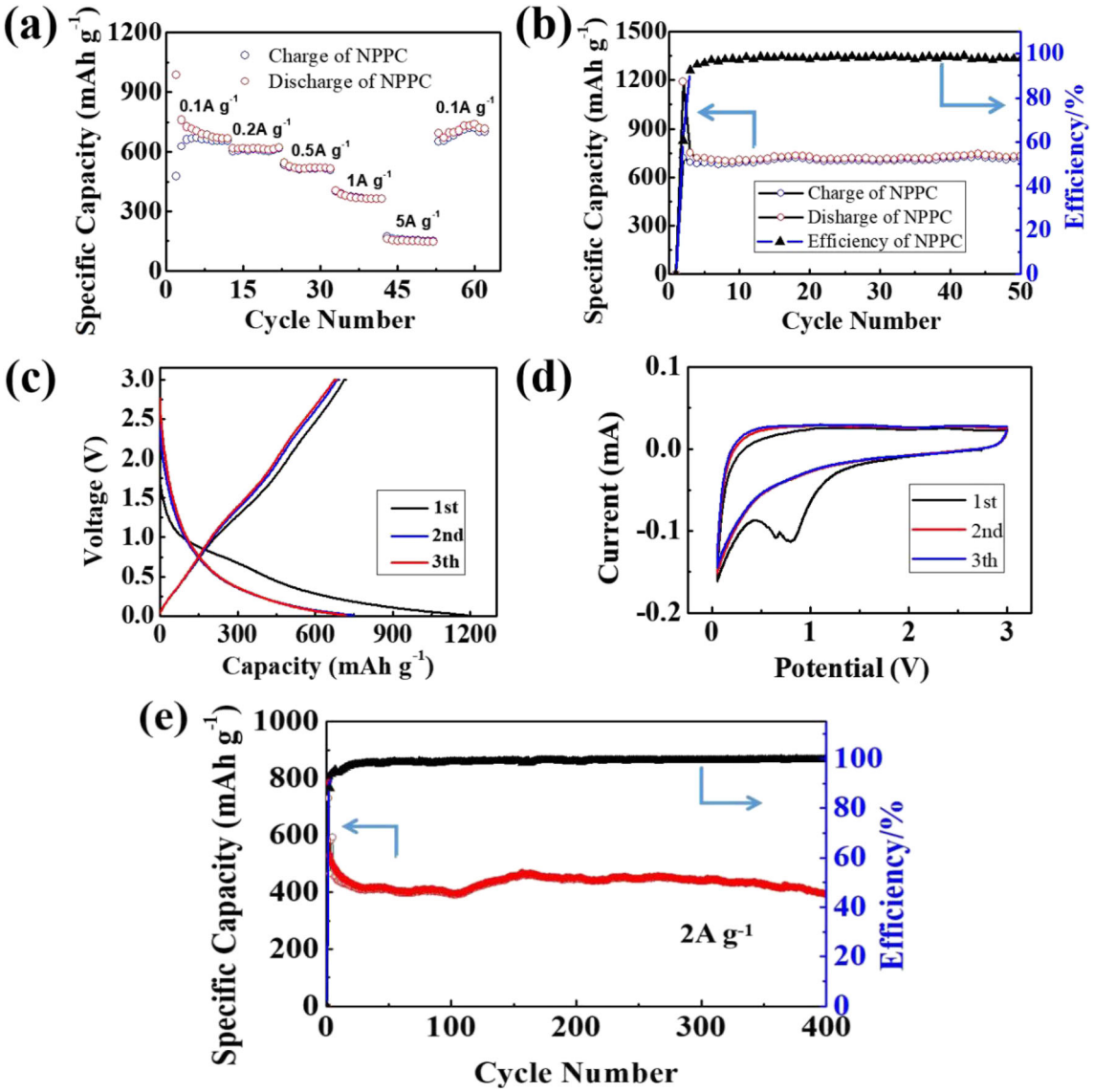

Fig. 4 **a** The rate performance of NPPC measured from different current densities. **b** The cycling performance and coulombic efficiency. **c** The initial-three charge/discharge curves of NPPC at 0.1 °C. **d** The cyclic voltammogram curves of NPPC. **e** The long cycling performance of NPPC at 2 A g^{-1} in the voltage range of 0.005–3.0 V

means that the oxidation of some SEI components is reversible and the capability decay mainly occurs in the first cycle. On the other hand, it also confirms that the electrode has good cycling stability and excellent reversibility [57]. Figure 4 e is a long cycle stability test for the material that shows the capacity of NPPC remains at 394.1 mAh g^{-1} after 400 cycles when the current density is 2 A g^{-1}, reaching 50.16% of the initial capacity. With the exception of a few cycles, the coulomb efficiency of NPPC remains above 99.5%. This further indicates that NPPC has good long period stability and structural stability.

EIS test is carried out to further research the dynamic information of NPPC materials in the frequency range from 10^{-3} to 10^{5} Hz at 0.005 V, and the Nyquist plot of the prepared sample is shown in Fig. 5. It shows that the impedance spectra curve consists of a semicircle and an inclined line. This was demonstrated in a number of studies that a semicircle at the high-to-medium frequencies on behalf of the double layer capacitance (CPE_2) and the resistance of charge transfer (R_{ct}), whereas the oblique line, which represents the Warburg impedance (Z_w), is associated with the diffusion of lithium ions in the electrode material. Besides, the inherent internal resistance (R_s) of the battery is derived from the electrode, electrolyte, and separator [50, 58, 59]. In Fig. 5, the insertion part is the simplified equivalent circuit model, and symbols correspond to the experimental data while the consecutive line is related to the fitting curves. It can be seen that the results of simulations are in a good agreement with measured values.

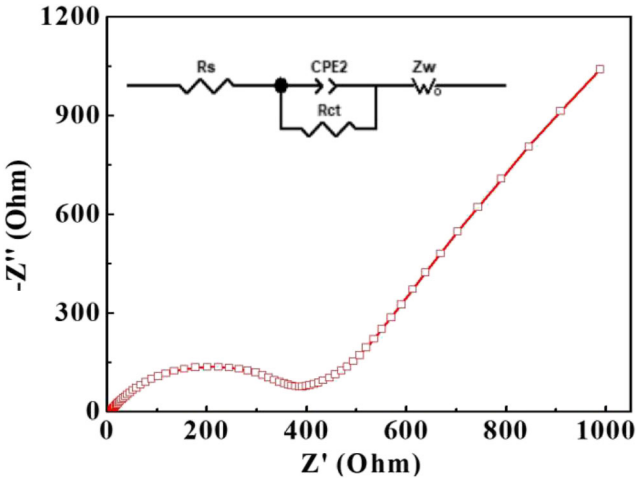

Fig. 5 Nyquist plots with the frequency range of 10^{-3}–10^{5} Hz for the NPPC samples and the corresponding result of simulation (inset is the equivalent circuit used for fitting an experimental curve)

From the above results, it can be seen that NPPC materials have excellent electrochemical properties, which can be attributed to the following points: (1) Porous carbon is not only conducive to the diffusion of lithium ions and the transfer of charge but also provides a larger contact area between the electrode and electrolyte, thus achieving higher specific capacity and good cycling performance. (2) Nitrogen doping can effectively be of help to improve the transport kinetics of lithium, provide more active sites and stable interfaces for lithium storage, thus improving the reversible capacity, rate performance, and cycling stability. (3) Additional P doping, on the one hand, enhances charge delocalization of carbon atoms, thus promoting charge separation and improving conductivity. On the other hand, carbon structures with many marginal sites are produced. (4) Nitrogen and phosphorus co-doping cause the binding energy of carbon-carbon bond to shift forward. The increase in binding energy means that more charges are transferred from carbon atoms to nearby N and P atoms, which can play an important role in improving the capacitive properties of materials.

Conclusion

To sum up, we successfully prepared the NPPC material with a simple method and studied its performance as a cathode material for lithium ion batteries. KCl and $ZnCl_2$ were used as salt templates to successfully prepare the porous carbon morphology. Using ionic liquid as carbon source and dopants that N and P elements were successfully doped. Electrochemical experiments show that NPPC has excellent specific capacity, rate, and cyclic stability. Therefore, NPPC is a promising anode material for lithium batteries. This work provides a novel method for the preparation of porous carbon materials mixed with nitrogen and phosphorus simultaneously and uniformly.

Funding The authors received financial support from the National Natural Science Foundation of China (NFSC) (grant nos. 52064035, 51404124). This work was supported by the fund of the State Key Laboratory of Advanced Processing and Recycling of Non-ferrous Metals, Lanzhou University of Technology (SKLAB02019015).

Compliance with ethical standards

Conflicts of interest The authors declare that they have no conflict of interest.

References

1. Li XM, Wolden CA, Ban CM, Yang YA (2015) Facile synthesis of lithium sulfide nanocrystals for use in advanced rechargeable batteries. ACS Appl Mater Interfaces **7**(51):28444–28451
2. Liang YR, Chen LY, Cai LF, Liu H, Fu RW, Zhang MQ, Wu DC (2016) Strong contribution of pore morphology to the high-rate electrochemical performance of lithium-ion batteries. Chem Commun (Camb) **52**(4):803–806
3. Raccichini R, Varzi A, Wei D, Passerini S (2017) Critical insight into the relentless progression toward graphene and graphene-containing materials for lithium-ion battery anodes. Adv Mater **29**(11)
4. Xu QS, Yang XF, Rao MM, Lin DC, Yan K, Du RA, Xu JT, Zhang YG, Ye DQ, Yang SH, Zhou GM, Lu YY, Qiu YC (2020) High energy density lithium metal batteries enabled by a porous graphene/MgF2 framework. Energy Storage Mater **26**:73–82
5. Bai J, Xi BJ, Mao HZ, Lin Y, Ma XJ, Feng JK, Xiong SL (2018) One-step construction of N,P-codoped porous carbon sheets/CoP hybrids with enhanced lithium and potassium storage. Adv Mater **30**(35):1802310
6. Wang HG, Yuan CP, Zhou R, Duan Q, Li YH (2017) Self-sacrifice template formation of nitrogen-doped porous carbon microtubes towards high performance anode materials in lithium ion batteries. Chem Eng J **316**:1004–1010
7. Li XN, Zhu XB, Zhu YC, Yuan ZQ, Si LL, Qian YT (2014) Porous nitrogen-doped carbon vegetable-sponges with enhanced lithium storage performance. Carbon **69**:515–524
8. Joshi BN, An S, Jo HS, Song KY, Park HG, Hwang S, Al-Deyab SS, Yoon WY, Yoon SS (2016) Flexible, freestanding, and binder-free SnO(x)-ZnO/carbon nanofiber composites for lithium ion battery anodes. ACS Appl Mater Interfaces **8**(14):9446–9453
9. Chen MH, Liu JL, Chao DL, Wang J, Yin JH, Lin JY, Jin Fan H, Xiang Shen Z (2014) Porous α-Fe 2 O 3 nanorods supported on carbon nanotubes-graphene foam as superior anode for lithium ion batteries. Nano Energy **9**:364–372
10. Zhang KL, Li XN, Liang JW, Zhu YC, Hu L, Cheng QS, Guo C, Lin N, Qian YT (2015) Nitrogen-doped porous interconnected double-shelled hollow carbon spheres with high capacity for lithium ion batteries and sodium ion batteries. Electrochim Acta **155**:174–182
11. Zhang X, Han SC, Xiao PA, Fan CL, Zhang WH (2016) Thermal reduction of graphene oxide mixed with hard carbon and their high performance as lithium ion battery anode. Carbon **100**:600–607
12. Lee J, Kim J, Hyeon T (2006) Recent progress in the synthesis of porous carbon materials. Adv Mater **18**(16):2073–2094
13. Shen XY, Chen S, Mu DB, Wu BR, Wu F (2013) Novel synthesis and electrochemical performance of nano-structured composite

with Cu2O embedment in porous carbon as anode material for lithium ion batteries. J Power Sources **238**:173–179
14. Yan Y, Yin YX, Xin S, Guo YG, Wan LJ (2012) Ionothermal synthesis of sulfur-doped porous carbons hybridized with graphene as superior anode materials for lithium-ion batteries. Chem Commun (Camb) **48**(86):10663–10665
15. Guo DC, Han F, Lu AH (2015) Porous carbon anodes for a high capacity lithium-ion battery obtained by incorporating silica into benzoxazine during polymerization. Chemistry **21**(4):1520–1525
16. Libbrecht W, Verberckmoes A, Thybaut JW, Van Der Voort P, De Clercq J (2017) Soft templated mesoporous carbons: tuning the porosity for the adsorption of large organic pollutants. Carbon **116**:528–546
17. Inagaki M, Toyoda M, Soneda Y, Tsujimura S, Morishita T (2016) Templated mesoporous carbons: synthesis and applications. Carbon **107**:448–473
18. Jia DD, Yu X, Tan H, Li XQ, Han F, Li LL, Liu H (2017) Hierarchical porous carbon with ordered straight micro-channels templated by continuous filament glass fiber arrays for high performance supercapacitors. J Mater Chem A **5**(4):1516–1525
19. Han BH, Zhou W, Sayari A (2003) Direct preparation of nanoporous carbon by nanocasting. J Am Chem Soc **125**(12): 3444–3445
20. Liang CD, Dai S (2006) Synthesis of mesoporous carbon materials via enhanced hydrogen-bonding interaction. J Am Chem Soc **128**(16):5316–5317
21. Zhou K, Hu MX, He Y, Yang L, Han CP, Lv RT, Kang FY, Li BH (2018) Transition metal assisted synthesis of tunable pore structure carbon with high performance as sodium/lithium ion battery anode. Carbon **129**:667–673
22. Hou JH, Cao CB, Idrees F, Ma XL (2015) Hierarchical porous nitrogen-doped carbon nanosheets derived from silk for ultrahigh-capacity battery anodes and supercapacitors. ACS Nano **9**(3):2556–2564
23. Jiang JG, Chen H, Wang Z, Bao LK, Qiang YW, Guan SY, Chen JD (2015) Nitrogen-doped hierarchical porous carbon microsphere through KOH activation for supercapacitors. J Colloid Interface Sci **452**:54–61
24. Paraknowitsch JP, Thomas A (2013) Doping carbons beyond nitrogen: an overview of advanced heteroatom doped carbons with boron, sulphur and phosphorus for energy applications. Energy Environ Sci **6**(10):2839
25. Wang HB, Maiyalagan T, Wang X (2012) Review on recent progress in nitrogen-doped graphene: synthesis, characterization, and its potential applications. ACS Catal **2**(5):781–794
26. Niu HJ, Zhang L, Feng JJ, Zhang QL, Huang H, Wang AJ (2019) Graphene-encapsulated cobalt nanoparticles embedded in porous nitrogen-doped graphitic carbon nanosheets as efficient electrocatalysts for oxygen reduction reaction. J Colloid Interface Sci **552**:744–751
27. Chen TQ, Pan LK, Loh TA, Chua DH, Yao YF, Chen Q, Li DS, Qin W, Sun Z (2014) Porous nitrogen-doped carbon microspheres as anode materials for lithium ion batteries. Dalton Trans **43**(40): 14931–14935
28. Cai DD, Wang CS, Shi CY, Tan N (2018) Facile synthesis of N and S co-doped graphene sheets as anode materials for high-performance lithium-ion batteries. J Alloys Compd **731**:235–242
29. Choi CH, Park SH, Woo SI (2012) Binary and ternary doping of nitrogen, boron, and phosphorus into carbon for enhancing electrochemical oxygen reduction activity. ACS Nano **6**(8):7084–7091
30. Wang CL, Zhou Y, Sun L, Wan P, Zhang X, Qiu JS (2013) Sustainable synthesis of phosphorus- and nitrogen-co-doped porous carbons with tunable surface properties for supercapacitors. J Power Sources **239**:81–88
31. Jiang HL, Zhu YH, Feng Q, Su YH, Yang XL, Li CZ (2014) Nitrogen and phosphorus dual-doped hierarchical porous carbon foams as efficient metal-free electrocatalysts for oxygen reduction reactions. Chem Eur J **20**(11):3106–3112
32. Yang DS, Bhattacharjya D, Inamdar S, Park J, Yu JS (2012) Phosphorus-doped ordered mesoporous carbons with different lengths as efficient metal-free electrocatalysts for oxygen reduction reaction in alkaline media. J Am Chem Soc **134**(39):16127–16130
33. Zhang N, Liu F, Xu SD, Wang FY, Yu Q, Liu L (2017) Nitrogen–phosphorus co-doped hollow carbon microspheres with hierarchical micro–meso–macroporous shells as efficient electrodes for supercapacitors. J Mater Chem A **5**(43):22631–22640
34. Du MQ, Meng YS, Wang C, Duan CY, Zhu FL, Zhang Y (2019) A simple synthesis of nitrogen-sulfur co-doped porous carbon using ionic liquids as dopant for high rate performance Li-ion batteries. J Electroanal Chem **834**:17–25
35. Qie L, Chen WM, Wang ZH, Shao QG, Li X, Yuan LX, Hu XL, Zhang WX, Huang YH (2012) Nitrogen-doped porous carbon nanofiber webs as anodes for lithium ion batteries with a superhigh capacity and rate capability. Adv Mater **24**(15):2047–2050
36. Wu ZS, Ren W, Xu L, Li F, Cheng HM (2011) Doped graphene sheets as anode materials with superhigh rate and large capacity for lithium ion batteries. ACS Nano **5**(7):5463–5471
37. Jawhari T, Roid A, Casado J (1995) Raman spectroscopic characterization of some commercially available carbon black materials. Carbon **33**(11):1561–1565
38. Reichardt S (2017) Wirtz L Raman spectroscopy of graphene. 85-132
39. Xiao MJ, Meng YS, Duan CY, Zhu FL, Zhang Y (2018) Nitrogen doped porous onion carbon derived from ionic liquids as the anode materials for lithium ion batteries with high performance. J Electroanal Chem **827**:167–174
40. Ou JK, Yang L, Zhang YZ, Chen L, Guo Y, Xiao D (2015) Fabrication of porous nitrogen-doped carbon materials as anodes for high-performance lithium ion batteries. Chin J Chem **33**(11): 1293–1302
41. Ma XL, Ning GQ, Qi CL, Xu CG, Gao JS (2014) Phosphorus and nitrogen dual-doped few-layered porous graphene: a high-performance anode material for lithium-ion batteries. ACS Appl Mater Interfaces 6(16):14415–14422
42. Han FD, Bai YJ, Liu R, Yao B, Qi YX, Lun N, Zhang JX (2011) Template-free synthesis of interconnected hollow carbon nanospheres for high-performance anode material in lithium-ion batteries. Adv Energy Mater **1**(5):798–801
43. Yang W, Yang W, Ding F, Sang L, Ma ZP, Shao GJ (2017) Template-free synthesis of ultrathin porous carbon shell with excellent conductivity for high-rate supercapacitors. Carbon **111**:419–427
44. Thommes M, Kaneko K, Neimark AV, Olivier JP, Rodriguez-Reinoso F, Rouquerol J, Sing KSW (2015) Physisorption of gases, with special reference to the evaluation of surface area and pore size distribution (IUPAC Technical Report). Pure Appl Chem **87**(9-10): 1051–1069
45. Zhu YD, Huang Y, Chen C, Wang MY, Liu PB (2019) Phosphorus-doped porous biomass carbon with ultra-stable performance in sodium storage and lithium storage. Electrochim Acta **321**:134698
46. Zhao H, Hu ZP, Zhu YP, Ge L, Yuan ZY (2019) P-doped mesoporous carbons for high-efficiency electrocatalytic oxygen reduction. Chin J Catal **40**(9):1366–1374
47. Sheng LZ, Jiang H, Liu SP, Chen MH, Wei T, Fan ZJ (2018) Nitrogen-doped carbon-coated MnO nanoparticles anchored on interconnected graphene ribbons for high-performance lithium-ion batteries. J Power Sources **397**:325–333
48. Yan XD, Liu Y, Fan XR, Jia XL, Yu YH, Yang XP (2014) Nitrogen/phosphorus co-doped nonporous carbon nanofibers for high-performance supercapacitors. J Power Sources **248**:745–751

49. Xu Y, Mo YP, Tian J, Wang P, Yu HG, Yu JG (2016) The synergistic effect of graphitic N and pyrrolic N for the enhanced photocatalytic performance of nitrogen-doped graphene/TiO2 nanocomposites. Appl Catal B Environ **181**:810–817
50. Wang HB, Zhang CJ, Liu ZH, Wang L, Han PX, Xu HX, Zhang KJ, Dong SM, Yao JH, Cui GL (2011) Nitrogen-doped graphene nanosheets with excellent lithium storage properties. J Mater Chem **21**(14):5430
51. Jiang XB, Shi HF, Shen JY, Han WQ, Sun XY, Li JS, Wang LJ (2018) Synergistic effect of pyrrolic N and graphitic N for the enhanced nitrophenol reduction of nitrogen-doped graphene-modified cathode in the bioelectrochemical system. J Electroanal Chem **823**: 32–39
52. Patel MA, Luo F, Khoshi MR, Rabie E, Zhang Q, Flach CR, Mendelsohn R, Garfunkel E, Szostak M, He H (2016) P-doped porous carbon as metal free catalysts for selective aerobic oxidation with an unexpected mechanism. ACS Nano **10**(2):2305–2315
53. Yang W, Yang W, Kong LN, Song AL, Qin XJ, Shao GJ (2018) Phosphorus-doped 3D hierarchical porous carbon for high-performance supercapacitors: a balanced strategy for pore structure and chemical composition. Carbon **127**:557–567
54. Zhu YY, Chen MM, Li Q, Yuan C, Wang CY (2018) A porous biomass-derived anode for high-performance sodium-ion batteries. Carbon **129**:695–701
55. Yang SB, Huo JP, Song HH, Chen XH (2008) A comparative study of electrochemical properties of two kinds of carbon nanotubes as anode materials for lithium ion batteries. Electrochim Acta **53**(5): 2238–2244
56. Mao Y, Duan H, Xu B, Zhang L, Hu YS, Zhao CC, Wang ZX, Chen LQ, Yang YS (2012) Lithium storage in nitrogen-rich mesoporous carbon materials. Energy Environ Sci **5**(7):7950
57. Zheng FC, Yang Y, Chen QW (2014) High lithium anodic performance of highly nitrogen-doped porous carbon prepared from a metal-organic framework. Nat Commun **5**:5261
58. Liu YY, Gu JJ, Zhang JL, Yu F, Dong LT, Nie N, Li W (2016) Metal organic frameworks derived porous lithium iron phosphate with continuous nitrogen-doped carbon networks for lithium ion batteries. J Power Sources **304**:42–50
59. Li YZ, Meng YS, Liu XL, Xiao MJ, Hu QR, Li RN, Ke XY, Ren GF, Zhu FL (2019) Double-protected zinc ferrite nanospheres as high rate and stable anode materials for lithium ion batteries. J Power Sources **442**:227256